THE TEMPERATURE AND DENSITY STRUCTURE OF AN Hα FLARING LOOP

M. D. DING, Y. LIU and P. F. CHEN
Department of Astronomy, Nanjing University, Nanjing 210093, China

(Received 18 July 2001; accepted 6 December 2001)

Abstract. We develop a simple method to deduce the temperature and density in the loop of a limb flare from the spectral observations of two lines, Hα and Ca II 8542 Å. We first build a grid of homogeneous slab models with various temperature and density values and compute the emergent line intensities, and then find the relevant model that can match the observed intensities. This is an approximate method because there are several other factors which can influence the line intensities. We apply this method to the limb flare of 11 November 1998 and deduce the values of temperature and hydrogen number density at different spatial points in the flaring loop, as well as their temporal variations. The loop contains relatively high density and possibly the loop top is slightly hotter and more condensed than the legs of the loop at the flare maximum time. A favorable scenario to produce this result is that magnetic reconnection occurs above the loop, and the reconnection outflow may heat and condense the plasma near the loop top.

1. Introduction

Flares are believed to occur through magnetic reconnection. The energy released in the reconnection site, in the form of either high-energy particles or a heat conduction front, can be transported downward to heat the chromosphere. The chromospheric material is then evaporated to the corona, filling the soft X-ray loop. The soft X-ray loop cools through radiation to finally an Hα loop, in a time which is dependent on the loop density. The spatial and temporal correlation between soft X-ray and Hα loops has been extensively studied by Schmieder *et al.* (1995, 1996), Wiik *et al.* (1996), and van Driel-Gesztelyi *et al.* (1997).

Recently, Chen *et al.* (1999) demonstrated through numerical simulations that the altitude of the reconnection site has an impact on the flare types. If the reconnection occurs in a relatively high place, the kinetic evolution of the flaring loops is qualitatively consistent with that predicted by a two-ribbon flare model (Kopp and Pneuman, 1976); while if the reconnection occurs in a relatively low place, the flare appears more likely to be a confined flare. It can be expected that the flaring loop in the latter case usually lies lower and contains a higher mass density than in the former case.

The physical conditions along the loop are of special interest since they might provide a constraint on the flare models. Masuda *et al.* (1994) found a hard X-ray source above the loop top and proposed that it is generated from the place where

Solar Physics **207:** 125–135, 2002.

a fast shock, emanating from the reconnection site, collides with the closed loop. Ranns *et al.* (2000) found for a flare that the non-thermal broadening of soft X-ray lines is located in and above soft X-ray loops. They suggested that it is due to either evaporating chromospheric plasma or plasma above the loop that is associated with the flare energy release. Ding *et al.* (1999) presented two-dimensional Hα spectra of a limb flare which show that the Hα line is most broadened at the loop top. The above facts highlight the special physical status at the loop top, which deserves to be studied further.

The 2D spectra of both Hα and Ca II 8542 Å for a limb flare of 11 November 1998, observed by the solar tower of Nanjing University (Huang *et al.*, 1995), provide an opportunity to study the physical condition along the flaring loop and its temporal variation. Ding *et al.* (1999) have argued that while the Hα line is optically thick, its broadening cannot be purely explained by the line opacity effect. The line broadening is more probably due to macro- and micro-turbulent velocities, or due to the bombardment of the atmosphere by non-thermal electron beams (Fang, Hénoux, and Ding, 2000). This work aims to derive the temperature and density values in the loop from the integrated intensities of the two lines based on non-LTE calculations for simple slab models. We finally discuss results in terms of current flare models.

2. The Observational Data

The flare occurred at the northwest limb (N25 W86) on 11 November 1998. It started at 02:10 UT, peaked at 02:15 UT, and ended at 02:18 UT. Its Hα/soft X-ray importance is SF/C3.2. We used the imaging spectrograph at the solar tower of Nanjing University to scan over the flaring region. Observations yielded 2D spectra of the Hα and Ca II 8542 Å lines. A detailed description of the observations and data reduction can be found in Ding *et al.* (1999).

We select 12 scans, covering the rise and decay phases of the Hα flaring loop, for study in this paper. The images at different times are co-aligned carefully using the sunspot and limb features near the flare. The accuracy of image co-alignment is estimated to be $2''-3''$. In the flaring loop, we select 3 points, which lie at the loop top and in the two legs, respectively, to check the spatial variation. Figure 1 shows a monochromatic image of the flaring loop at Hα line center at 02:14:38 UT and the selected points in the loop.

3. The Numerical Method

Inversion of line profiles has been an attractive topic in the spectral analysis of solar features for many years, but only recently was non-LTE inversion tackled. Socas-Navarro, Ruiz Cobo, and Trujillo Bueno (1998) developed a non-LTE inversion

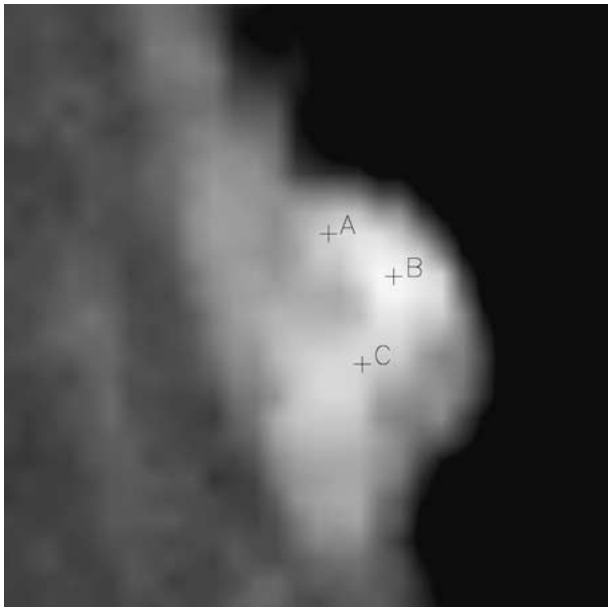

Figure 1. A monochromatic image of the flaring loop at Hα line center at 02:14:38 UT, reconstructed from the 2D spectra obtained by a scanning technique. The field of view is $45'' \times 45''$. The spatial positions of the three points extracted for further study are marked in the loop.

code of spectral lines, based on the concept of response functions (e.g., Mein, 1971) and the fixed departure coefficients (FDC) approximation. This method is able to recover the thermodynamical variables in the solar atmosphere. An alternative way for spectral line inversion is first to compute a large grid of models (the database) that cover the possible range of physical parameters and then to search for the model that can best reproduce the observed profiles (Molowny-Horas *et al.*, 1999; Tziotziou *et al.*, 2001; Rees *et al.*, 2000). To avoid a very big database, this method is better used in simple features with only a few free parameters, like filaments and prominences, etc. However, it becomes an efficient way when inverting a large number of profiles. In this paper, we use a similar method to this to deduce the temperature and density within the loop of the limb flare by adopting a simple slab model.

3.1. SLAB MODEL

Solar features that extend over the limb can be simply modeled as vertical slabs of finite width. This method has been used to study the formation of spectral lines in prominences or post-flare loops under non-LTE conditions (e.g., Heinzel, Schmieder, and Mein, 1992; Gouttebroze, Heinzel, and Vial, 1993). For the case studied here, we take a slab width of 3000 km, which is comparable to the diameter of the flaring loop. The temperature and mass density can be treated as

constant along the loop width (the line of sight). For simplicity, we do not include a detailed transition region between the loop structure and the corona, as was done by Schmieder *et al.* (1999) when analyzing the Lyman lines in a quiescent prominence, but instead consider an incident radiation field to both surfaces of the slab. The irradiation intensity is taken to be half the mean intensity from the solar surface.

Neglect of a loop–corona transition region yields an inaccurate assessment of the incident EUV radiation which determines the transition rates in the hydrogen Lyman series in surface layers. But it should have no great influence on the Hα line, since in the best case which can reproduce the observed line intensities this line is extremely opaque. Moreover, the EUV irradiation has no direct influence on the Ca II 8542 Å line.

3.2. Computational procedure

We first make non-LTE calculations for the slab model and obtain the line profiles of Hα and Ca II 8542 Å under different conditions by varying the slab temperature (T) and hydrogen number density (n_H). We then integrate the line intensities with respect to wavelength to get the integrated intensities as a two-dimensional function of T and n_H. By comparing the observed and computed integrated intensities, which are denoted by superscripts 'o' and 'c', respectively,

$$I^{\mathrm{o}}_{\mathrm{H}\alpha} = I^{\mathrm{c}}_{\mathrm{H}\alpha}(T, n_H), \tag{1}$$

$$I^{\mathrm{o}}_{\lambda 8542} = I^{\mathrm{c}}_{\lambda 8542}(T, n_H), \tag{2}$$

we then search for a solution of T and n_H which can serve as a mean physical condition in the loop where the observed lines are formed. In most cases, Equations (1) and (2) yield a unique solution.

Our searching box covers a range of $6000 < T < 16\,000$ K and $10^{11} < n_H < 10^{13}$ cm^{-3}. Within this range, the integrated intensity of the Hα line is found to increase monotonically with increasing T. The intensity of the Ca II 8542 Å line, however, is not a monotonic function of T; it increases first, peaks at a temperature which is dependent on the loop density, and then decreases with increasing T. Both the intensity of Hα and that of Ca II 8542 Å increase with n_H, but the relation is not linear, especially when the lines are optically thick.

4. Influence of Other Factors

Besides the temperature and density, there are several other factors which can influence the line intensity. The most significant ones are the electron beam bombardment, the incident radiation, the micro-turbulent velocity and the macroscopic velocity. A macroscopic velocity can produce the effect of Doppler-brightening or

Doppler-dimming (e.g., Heinzel and Rompolt, 1987). However, since the loop may actually contain many fine structures with dispersive macro-velocities (Ding *et al.*, 1999), it is hard to judge how the macro-velocities can influence the line intensity. Therefore, here we check the effect of the first three factors. In the following computations, we start from the reference parameters: a micro-turbulent velocity of 10 km s^{-1}, an incident radiation from a quiet-Sun atmosphere, and no electron beam bombardment, and then change one of the three factors to test its impact on the line intensities.

4.1. Effect of electron beam bombardment

The flaring loop may be heated by a non-thermal electron beam. The Hα loop is believed to originate from the cooling of the hot (soft X-ray) loop. The cooling time depends on the loop density. For the present case, the hydrogen number density is inferred to be greater than 10^{12} cm^{-3}, which yields a relatively short cooling time (several tens of seconds). Therefore, it is possible that the electron beam heating continues to exist in the cool (Hα) loop. Such an electron beam can cause non-thermal excitation and ionization of the atoms and change the radiation from the loop (e.g., Fang, Hénoux, and Gan, 1993).

To quantitatively check this effect, we also do calculations for the case that the loop (the model slab) is bombarded vertically by a uniform electron beam with an energy flux of $\mathcal{F} = 10^{10}$ erg cm^{-2} s^{-1}. The column density between the source of the beam and the loop is assumed to be 0.001 g cm^{-2}. Figure 2 plots the integrated intensities of Hα and Ca II 8542 Å as functions of temperature and density, in the two cases with and without the electron beam. We find that the non-thermal effect is quite efficient in raising the Hα intensity in the lower temperature domain ($T \lesssim 10^4$ K), while this effect becomes negligible when the temperature goes higher and thermal excitation/ionization dominates. For the Ca II 8542 Å line, its intensity is also enhanced in case of a relatively low temperature; however, the intensity is reduced somewhat around a temperature which yields maximum emission. This is due to the fact that the Ca II 8542 Å line is optically thin or marginally optically thin and the non-thermal effect reduces further the opacity of the line although the line source function may be increased.

4.2. Effect of micro-turbulent velocity

The flaring atmosphere is very dynamic and turbulent, especially during the peak time. A micro-turbulent velocity redistributes the absorption coefficient and makes the line center less opaque but the line wings more opaque. Usually this favors increasing the integrated line intensity. Figure 3 compares the integrated intensities computed in two cases with micro-turbulent velocities of 10 and 15 km s^{-1}, respectively. The difference is noticeable. A micro-turbulent velocity larger than 15 km s^{-1} is unreasonable since it exceeds the local acoustic speed in a loop with a temperature around 10^4 K.

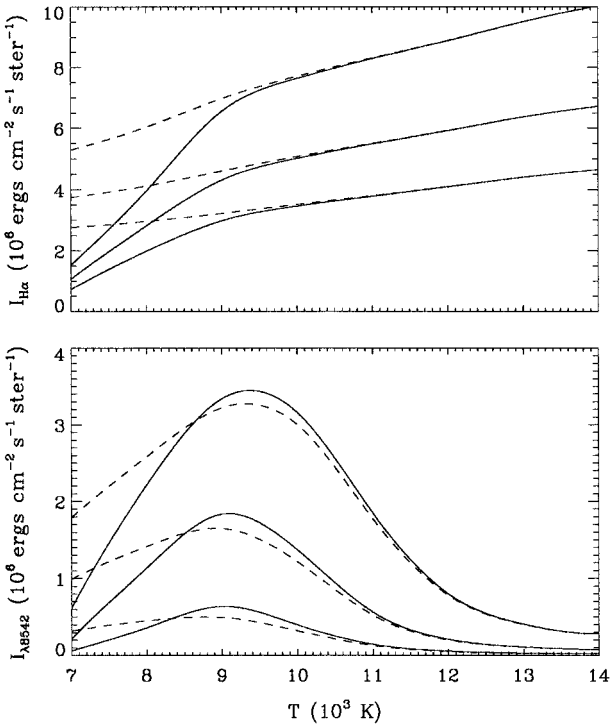

Figure 2. Integrated intensities of Hα and Ca II 8542 Å as functtions of temperature and density of the model slab, in the two cases with (*dashed lines*) and without (*solid lines*) the electron beam. In the former case, the beam flux is $\mathcal{F} = 10^{10}$ erg cm^{-2} s^{-1}. *From bottom to top*, the three sets of lines correspond to $n_H = 10^{12}$, 2×10^{12}, and 4×10^{12} cm^{-3}, respectively.

4.3. Effect of incident radiation

The incident radiation on the surfaces of the slab may change during the flaring process. A stronger incident radiation causes more excitation and ionization of the atoms in the slab and then yields a stronger emergent radiation. This effect is most important in an optically thin case. We plot in Figure 4 the integrated intensities in two cases of different incident radiation fields, which are computed from a quiet-Sun model atmosphere VAL-C (Vernazza, Avrett, and Loeser, 1981) and a flare model atmosphere F1 (Machado *et al.*, 1980), respectively. (Note that a dilution factor of 0.5 is assumed in both cases.) It shows that if the change of the incident radiation is within the range as specified here, its effect on the line intensities is much smaller than the other two factors described above.

To test how the above factors could influence the deduced results, we first compute the line intensities for some selected slab models by adopting the reference parameters, and then use them as artificial observed values and apply the procedure in Section 3.2 when changing one of the three parameters mentioned above. The results are shown in Figure 5. We find that assuming a non-thermal effect tends

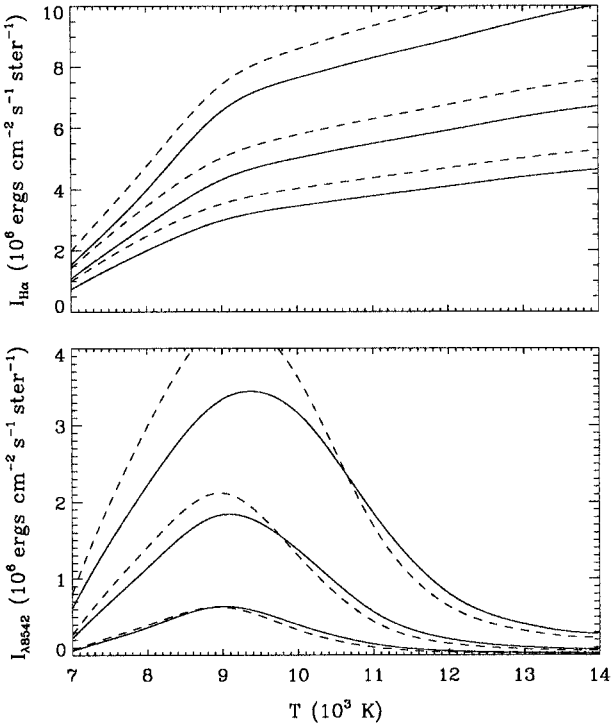

Figure 3. Integrated intensities of Hα and Ca II 8542 Å as functions of temperature and density of the model slab, in the two cases with micro-turbulent velocities of 10 (*solid lines*) and 15 (*dashed lines*) km s^{-1}. *From bottom to top*, the three sets of lines correspond to $n_H = 10^{12}$, 2×10^{12}, and 4×10^{12} cm^{-3}, respectively.

to lower the deduced temperature; however, this effect is obvious only when the temperature is $\lesssim 10^4$ K, which is beyond the temperature range that we derive for the flare studied here, as will be shown below. The effect of adopting a larger micro-turbulent velocity is mainly to lower the temperature value and also to lower the density value. The former is preferential in a case of relatively low density and the latter becomes obvious in a case of relatively high density. The effect of varying the incident radiation on the final results is small, as expected.

5. Application to the 11 November 1998 Limb Flare

We have applied the above method to the limb flare of 11 November 1998. For lack of sufficient knowledge about the non-thermal electron heating, micro-turbulent velocity, and incident radiation, we just adopt the reference parameters and neglect their temporal variation. The results are displayed in Figure 6.

It can be seen that all the three points selected underwent a temperature and density variation with the development of the flare. In the northern leg and at the

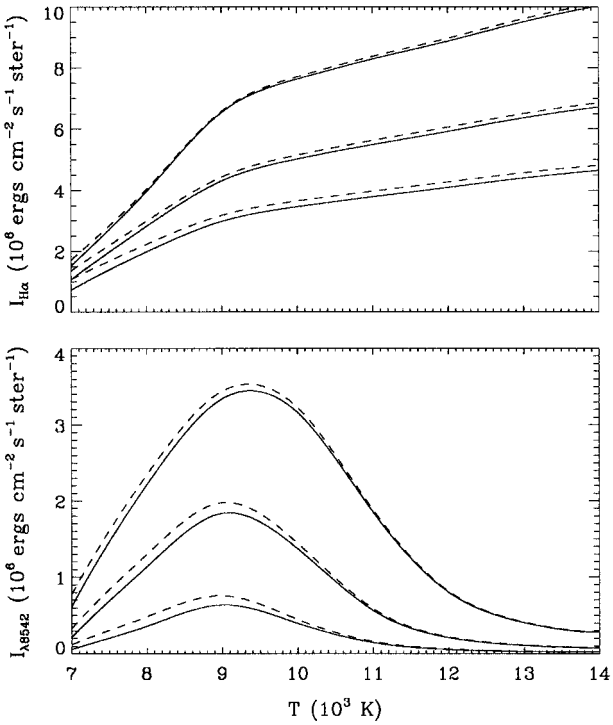

Figure 4. Integrated intensities of Hα and Ca II 8542 Å in dependence of temperature and density of the model slab, in the two cases of different incident radiation fields: one computed from the quiet-Sun model VAL-C (*solid lines*) and the other from the flare model F1 (*dashed lines*). *From bottom to top*, the three sets of lines correspond to $n_H = 10^{12}$, 2×10^{12}, and 4×10^{12} cm^{-3}, respectively.

loop top, the temperature and density peak at $\sim$ 02:14–02:15 UT, in coincidence with the Hα maximum; in the southern leg, however, the temperature and density peak before the first scan and show a gradual decreasing during the observing time. This difference could be interpreted as an asymmetric heating in one loop or a superposition of spatially unresolved loops in which the heating is not coincident.

The deduced temperature in the loop lies in the range of 10 000–12 500 K, which is a typical temperature in post-flare loops. The hydrogen number density varies in the range of $(1.0–3.5)\times 10^{12}$ cm^{-3}. This relatively high density implies a short cooling time of the loop from soft X-ray to Hα emitting temperatures. Under the present assumption that the loop can be mimicked by a slab with a uniform geometrical thickness, the loop top, during the flare maximum time, seems to contain a temperature and a density that both are slightly higher than the values in the legs of the loop. However, the difference is not large enough to make this point conclusive. As is shown above, there are other factors which can influence the deduced values of temperature and density. In particular, we mention the role of micro-turbulence, which is possibly varying along the loop instead of a constant as

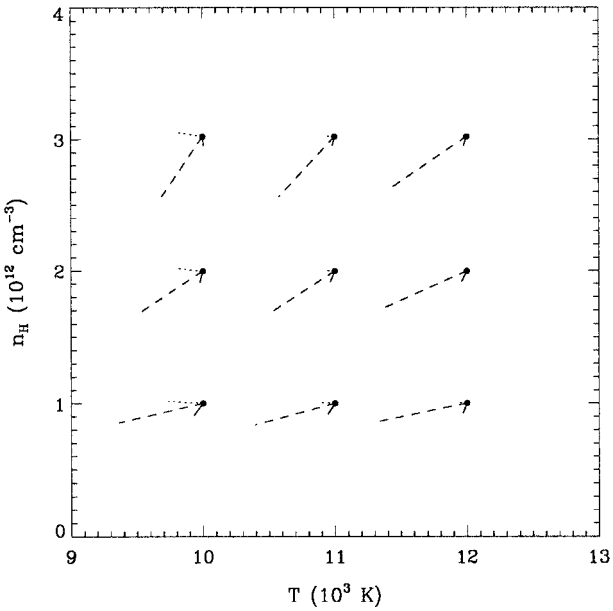

Figure 5. Influence of the three factors on the deduced results. The *filled circles* represent grid points of T and n_H where the line intensities are computed by adopting the reference parameters and are then used as an input to the procedure when one of the three parameters is changed. Change of the deduced values of T and n_H is depicted by the *dotted*, *dashed*, and *solid lines*, which represent the effect of assuming a non-thermal electron beam ($\mathcal{F} = 10^{10}$ erg cm^{-2} s^{-1}), that of adopting a larger micro-turbulent velocity of 15 km s^{-1}, and that of adopting an incident radiation field from a flare model atmosphere F1, respectively.

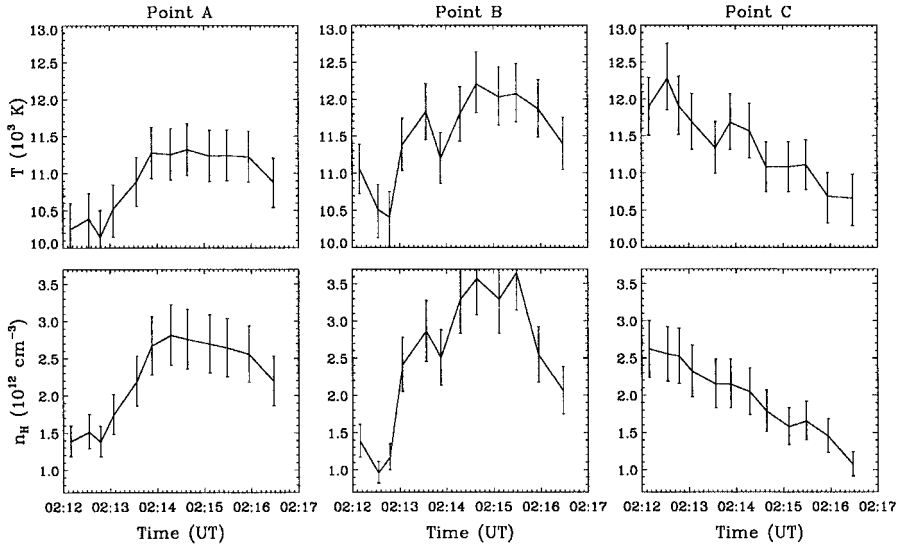

Figure 6. Temperature and hydrogen number density at the three points in the loop (see Figure 1) deduced through the method described here. We have assumed an uncertainty of ±10% in the calibration of absolute intensities of both lines.

assumed in the computations. In fact, assuming a larger micro-turbulent velocity at the loop top than in the legs can reduce such a difference. However, for the present event, it is hard to make a quantitative assessment of the spatial variation of micro-turbulence based on the observed data. Therefore, we need to study more events to test the above results, which, if established, can be interpreted in terms of the following scenario. Magnetic reconnection is supposed to occur above the flaring loop, and the outflow from the reconnection site impinges the closed loop to heat and condense the material there.

Finally, we note that the above method does not take into account the fine structures which may exist in the flaring loop, as was indicated by Ding *et al.* (1999). Therefore, the physical parameters derived above can only be regarded as mean values in the line-forming region.

6. Conclusions

Heating, cooling and radiation processes in a flaring loop are determined by the physical conditions within the loop. In this paper we develop a simple method to deduce the temperature and density in a limb flare from spectral observations of two lines, Hα and Ca II 8542 Å. We build a grid of homogeneous slab models with various temperature and density values and compute the emergent line intensities using a non-LTE code. The problem is thus to find the relevant model that can match the observed intensities of the two lines. This method is approximate in that there are several other factors which can influence the line intensities. We explore quantitatively the effect of non-thermal electron bombardment, micro-turbulent velocity, and incident radiation.

The method is applied to the limb flare of 11 November 1998. For simplicity, we adopt a constant micro-turbulent velocity and do not include the effect of non-thermal electron bombardment. We deduce the values of temperature and hydrogen number density at different spatial points in the flaring loop, as well as their temporal variations. It is found that the loop contains a relatively high density. In addition, the loop top seems slightly hotter and more condensed than the legs of the loop at the flare maximum time. More observations of limb flares are needed to check this point. A favorable scenario to produce this result is that magnetic reconnection occurs above the loop, and the reconnection outflow may heat and condense the plasma near the loop top.

Acknowledgements

We are grateful to the referee for valuable comments which helped to clarify some key points. This work was supported by TRAPOYT, NSFC under grant 10025315, and NKBRSF under grant G20000784.

References

Chen, P. F., Fang, C., Ding, M. D., and Tang, Y. H.: 1999, *Astrophys. J.* **520**, 853.
Ding, M. D., Fang, C., Yin, S. Y., and Chen, P. F.: 1999, *Astron. Astrophys.* **348**, L29.
Fang, C., Hénoux, J.-C., and Ding, M. D.: 2000, *Astron. Astrophys.* **360**, 702.
Fang, C., Hénoux, J.-C., and Gan, W. Q.: 1993, *Astron. Astrophys.* **274**, 917.
Gouttebroze, P., Heinzel, P., and Vial, J. C.: 1993, *Astron. Astrophys. Suppl. Ser.* **99**, 513.
Heinzel, P. and Rompolt, B.: 1987, *Solar Phys.* **110**, 171.
Heinzel, P., Schmieder, B., and Mein, P.: 1992, *Solar Phys.* **139**, 81.
Huang, Y. R., Fang, C., Ding, M. D., Gao, X. F., Zhu, Z. G., Ying, S. Y., Hu, J., and Xue, Y. Z.: 1995, *Solar Phys.* **159**, 127.
Kopp, R. A. and Pneuman, G. W.: 1976, *Solar Phys.* **50**, 85.
Machado, M. E., Avrett, E. H., Vernazza, J. E., and Noyes, R. W.: 1980, *Astrophys. J.* **242**, 336.
Masuda, S., Kosugi, T., Hara, H., Tsuneta, S., and Ogawara, Y.: 1994, *Nature* **371**, 495.
Mein, P.: 1971, *Solar Phys.* **20**, 3.
Molowny-Horas, R., Heinzel, P., Mein, P., and Mein, N.: 1999, *Astron. Astrophys.* **345**, 618.
Ranns, N. D. R., Matthews, S. A., Harra, L. K., and Culhane, J. L.: 2000, *Astron. Astrophys.* **364**, 859.
Rees, D. E., López Ariste, A., Thatcher, J., and Semel, M.: 2000, *Astron. Astrophys.* **355**, 759.
Schmieder, B., Heinzel, P., Wiik, J. E., Lemen, J., Anwar, B., Kotrč, P., and Hiei, E.: 1995, *Solar Phys.* **156**, 337.
Schmieder, B., Heinzel, P., van Driel-Gesztelyi, L., and Lemen, J. R.: 1996, *Solar Phys.* **165**, 303.
Schmieder, B., Heinzel, P., Vial, J. C., and Rudawy, P.: 1999, *Solar Phys.* **189**, 109.
Socas-Navarro, H., Ruiz Cobo, B., and Trujillo Bueno, J.: 1998, *Astrophys. J.* **507**, 470.
Tziotziou, K., Heinzel, P., Mein, P., and Mein, N.: 2001, *Astron. Astrophys.* **366**, 686.
van Driel-Gesztelyi, L., Wiik, J. E., Schmieder, B., Tarbell, T., Kitai, R., Funakoshi, Y., and Anwar, B.: 1997, *Solar Phys.* **174**, 151.
Vernazza, J. E., Avrett, E. H., and Loeser, R.: 1981, *Astrophys. J. Suppl. Ser.* **45**, 635.
Wiik, J. E., Schmieder, B., Heinzel, P., and Roudier, T.: 1996, *Solar Phys.* **166**, 89.